Nanomaterials and Nanotechnology

OPEN ACCESS
ARTICLE

Properties of Aluminosilicate Refractories with Synthesized Boron-Modified TiO_2 Nanocrystals

Regular Paper

Claudia Carlucci[1], Francesca Conciauro[2], Barbara Federica Scremin[2], Antonio Graziano Antico[2], Marco Muscogiuri[4], Teresa Sibillano[3], Cinzia Giannini[3], Emanuela Filippo[4], Caterina Lorusso[4], Paolo Maria Congedo[4]* and Giuseppe Ciccarella[2]*

1 Chemistry Department, University of Bari, Bari, Italy
2 National Nanotechnology Laboratory (NNL), Nanoscience Institute—CNR, Lecce, Italy
3 Institute of Crystallography (IC)—CNR, Bari, Italy
4 Department of Engineering for Innovation, University of Salento, Lecce, Italy
* Corresponding author(s) E-mail: giuseppe.ciccarella@unisalento.it; paolo.congedo@unisalento.it

Received 21 November 2014; Accepted 06 February 2015

DOI: 10.5772/60204

Abstract

An efficient microwave supported synthesis, with a reaction time of only one and a half minute, to prepare boron-modified titania nanocrystals TiO_2:(B), was developed. The nanocrystals were obtained by hydrolysis of titanium tetraisopropoxide (TTIP) together with benzyl alcohol and boric acid, and the approach did not need surfactants use and a final calcination step. The produced TiO_2:(B) nanocrystals were characterized in detail by low magnification Transmission Electron Microscopy (TEM), Inductively Coupled Plasma-Atomic Emission Spectroscopy (ICP-AES), X-Ray Diffractometry (XRD), and a Micro Raman Spectroscopy. One of the obtained samples was then tested as an additive in various amounts in a typical aluminosilicate refractory composition. The effects of these additions in bricks were evaluated, according to UNI EN 196/2005, in terms of thermo-physical and mechanical properties: diffusivity, bulk density, apparent density, open and apparent porosity and cold crushing strength. Bricks' microstructure was analysed by Scanning Electron Microscopy (SEM) and energy dispersion spectroscopy (EDS). The bricks obtained with nanoadditives presented improved mechanical characteristics with respect to the typical aluminosilicates, presumably because of a better compaction during the raw materials' mixing stage.

Keywords TiO_2, Anatase, Boron, Aluminosilicate, Nanocrystals, Refractories

1. Introduction

Aluminosilicate bricks have been used as refractory in industrial furnaces in constructing and restoring, in coke ovens, glass melting furnaces, and hot blast furnaces [1, 2]. The high temperature volume stability and creep features of aluminosilicate bricks [2] are the unique properties of the heavy-duty refractory products. The conventional silica bricks generally exhibit some disadvantages such as

degradation [1, 3], low refractoriness [4], and thermal expansion due to their poor alkali content and thermal resistance [5, 6, 7]. The incorporation of nano-metal oxides, such as TiO_2, enhances the physico-chemical and thermo-mechanical properties of refractories and their composites [8, 9, 10].

The processing of nanomaterials for the construction industry is complex in nature and requires careful monitoring to achieve the required performances. In the case of nanocomposites a major difficulty lies in the tendency of nanoparticles to aggregate into micrometer-sized crystalline forms in the attempt to reduce their surface free energy.

The present investigation deals with the eco-friendly production of nanoscale boron-modified TiO_2 particles and their application in aluminosilicate refractories. It is necessary, however, that the nanoparticles arrange uniformly in the matrix to effectively contribute to the composite's final properties; the nanoparticles' shape, moreover, may be important in increasing the compound mechanical strength according to preferential directions.

Knowledge of the thermo-mechanical properties of nanocrystals modified in an aluminosilicate refractory is relatively limited, and potentially of great importance, because such materials in service are typically subjected to constant stress over long periods, and therefore a design that ensures components' optimal performance over time requires a careful estimation of their lifetime.

In this paper concerned with improving thermal/insulating quality, resistance, and lifetime of standard concrete, boron-modified titanium dioxide nanoparticles were added to aluminosilicate specimens and the resultant thermo-physical and mechanical characterizations are presented. Tests were conducted also using anatase titanium dioxide nanocrystals synthesized in our previous works [11] but the results with boron modified anatase nanocrystals of the present study gave better results in terms of bricks' properties.

Physical properties, such as thermal diffusivity, apparent porosity, water absorption, and density were measured and compression mechanical resistance has been studied.

Finally, the open pore distribution and their size were estimated by mercury porosimetric analysis supporting the results from thermal and mechanical characterization. The refractories with and without additive (standard) were compared to highlight the changes in the composites' behaviour. Microstructure study was performed with SEM-EDS analysis.

2. Materials and methods

2.1 Synthesis

Ti(IV)-isopropoxide ($Ti(OPri)_4$ or TTIP, 97%), benzyl alcohol ($C_6H_5CH_2OH$ or BzOH, ≥99%), boric acid (H_3BO_3 99.5%), nitric acid, and hydrofluoric acid (HF 47-51% Hg <10 ppb) (HNO3 70% (Hg ≤0.0000005%) were purchased from Aldrich. The reagents were employed as received without additional purification.

In a typical preparation, TTIP (1 mL, 3.36 mmol) was added to boric acid dispersed in benzyl alcohol (10 mL, 96.4 mmol), while stirring in a Teflon vessel. The reaction vessel was sealed and maintained at 200° C for 1 minute and 30 seconds, without the requirement of a post-synthetic calcination treatment of the nanocrystals [12]. The microwave-assisted synthesis took place in a single and quick step, by using a microwave digestion system [13, 14, 15]. The system uses 2.45 GHz microwaves and it is controlled in both temperature (200 °C) and pressure (300 psi). The reaction vessel has been connected to a pressure transducer that monitors and controls the pressure during synthesis. The resulting milky suspension was centrifuged; the white precipitate was twice washed with diisopropylether and dried overnight at room temperature. Different TTIP: H_3BO_3 molar ratios (1:1, 1:2, 1:3, 1:4, 1:5) were tested and samples were named BT1, BT2, BT3, BT4, and BT5, respectively.

2.2 Preparation of aluminosilicate bricks

The BT2 nanocrystals were tested as bricks' additives. They were prepared in three different suspensions of benzyl alcohol in concentration percentages of 0.5 wt.%, 1 wt.%, and 2 wt.%.

The bricks were obtained mixing 2.2 kg of commercial refractory material (Al_2O_3 55 wt.% and SiO_2 42 wt.%) with water at 6 wt.% in which the additive suspensions were emulsified previously. The mixture was "thrown" in the mould in two different phases spaced by a compaction process and placed in the curing chamber at 20 °C, exposed to not less than 90% relative humidity for 24 hours; then each brick was carried out of the mould, and put back in the chamber to mature for 28 days, as described in UNI EN 196/2005. Later all the specimens were fired at 1300 °C for 24 hours.

2.3 Nanocrystals' characterization

Morphological characterizations of the TiO_2:(B) nanopowders were performed using a JEOL JEM 1011 Transmission Electron Microscope (TEM). Inductively Coupled Plasma-Atomic Emission Spectroscopy (ICP-AES) was performed on a Varian Vista AX ICP-AES instrument, with samples digested using a mixture of HNO_3 and HF 1:1. The ICP-AES measurements were accomplished by calibration using aqueous standards of Ti and B after appropriate dilution; the calibration ranges were selected according to the expected concentrations of the elements of interest.

The Raman spectra were acquired with a Renishaw inVia Raman microscope, with 633 nm excitation wavelength, a 50X microscope objective giving a spot diameter of 2μm, a resolution of 4 cm^{-1}, and a power of about 0.8 mW. Powders

of the prepared samples were placed on a glass slide, and spectra were collected at room temperature.

Powder X-ray diffraction (XRD) for phase analysis of the nanocrystals was performed on a Rigaku diffractometer in Bragg-Brentano reflection geometry, using filtered Cu Kα radiation. The XRD patterns were recorded in the range of 2Θ = 20° - 90° by step scanning, using 2Θ increments of 0.03° and a fixed counting time of 2 s/step.

The XRD patterns revealed only the presence of the anatase phase and were analysed by using a whole-profile Rietveld-based fitting program [16] according to the following procedure, fully described elsewhere [11–15]:

1. The instrumental resolution function (IRF) was evaluated by fitting the XRD pattern of a LaB6 NIST standard recorded under the same experimental conditions as those used for measuring the samples. The IRF data file was provided separately to the program in order to allow subsequent refinement of the XRD patterns of the samples.
2. The phase composition of the samples was determined by fitting the XRD patterns with the crystal structure models of tetragonal TiO_2 anatase (space group I41/amd; cell parameters: a = b = 3.7835430 Å and c = 9.614647 Å; $\alpha = \beta = \gamma = 90°$). The weight percentage accuracy of the estimation was determined to be 5–7% w/w.
3. The inhomogeneous peak broadening of the anatase TiO_2 reflections was described by a phenomenological model based on the modified Scherrer formula [11–15]. The refinement procedure allowed the calculation of the coherent crystal apparent domain size along each reciprocal lattice vector (h,k,l) direction. Other refinable parameters were the unit cell parameters, whereas the background was linearly interpolated and unrefined.

2.4 Aluminosilicate bricks' characterization

All bricks were characterized by different techniques. Density, apparent porosity, and water absorption were measured by the Archimedes method using water. Thermal diffusivity was determined using the Hot Disk technique: a disk sensor was placed between two pieces of the sample material, then heated by a constant electrical current for about 40 s. The generated heat, dissipated from the sensor into the surrounding unknown sample material, causes a temperature variation both in the sensor and in the surrounding material. The sensor average transient temperature is simultaneously measured monitoring a change in its electrical resistance. The sensor resistivity change correlates with the corresponding change in temperature through a temperature coefficient of resistivity.

The refractory mechanical performances were estimated by compression breaking tests, according to the Standard in force (UNI EN 196/2005); prismatic specimens were used (4x4x4 cm) and a 65-L12G2 Controls programmed control press was employed. The load was increased uniformly at a speed of 2400 N / s until specimen failure, which is of the brittle type.

The bricks' microstructure was analysed through Scanning Electron Microscopy with a JEOL 5410 LV SEM microscope equipped for energy dispersion spectroscopy (EDS). EDS allows detecting X-photons emitted by the sample in response to the incident electrons from the SEM microscope giving evidence about the specimen elemental composition. The samples were fractured under liquid nitrogen and successively metalized to ensure a good electrical conductivity.

Porosimetry measurements were accomplished with a Pascal 140 and 240 Thermo Finnigan mercury porosimeters. The penetration pressure relates directly to the pores' size according to the Washburn equation [17]:

$$R = -2\gamma\cos\theta / P_c$$

where γ is the mercury surface tension (generally 0.480 N/m), θ is the contact angle between the mercury and the solid (in average 140°), Pc is the penetration pressure, and R the pore radius. The hypothesis of the Washburn equation is that of cylindrical pores.

3. Results and discussion

TEM images of the boron-modified titania nanoparticles are reported in Figure 1.

TEM analysis, reported in Table 1, revealed that the axes' average lengths were comparable in all the samples, with an estimated average length for the short axis of about 5–6 nm, and of 7–8 nm for the long axis.

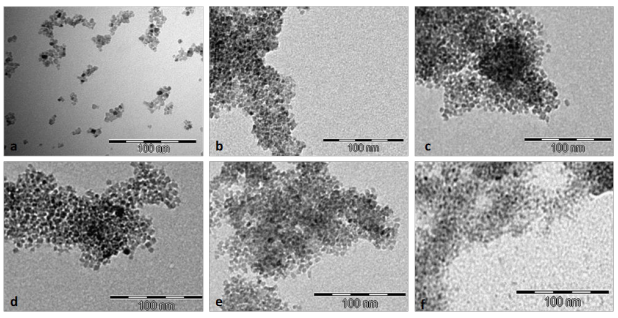

Figure 1. TEM images of the TiO_2:(B) nanoparticles synthesized with different TIIP:H3BO3 ratios. Undoped TiO_2 (a); BT1 (b); BT2 (c), BT3 (d), BT4 (e), and BT5 (f).

The calculated aspect ratios were comparable under the error in all the samples, thus boron addition did not influence appreciably the size of the resultant nanocrystals. Boron content evaluated by ICP-AES increased with the nominal increment of TiO_2: B ratio (Table 1).

Sample	Boric Acid (mmol) [a]	TiO_2: B Ratio [b]	B: Ti [c]	Long axis (nm) [d]	Short axis (nm) [d]	Aspect Ratio [e]
BT1	3.36	1:1	0.007	6.6 ± 1.0	5.0 ± 0.8	1.3 ± 0.3
BT2	6.72	1:2	0.020	7.0 ± 0.9	5.6 ± 0.7	1.2 ± 0.2
BT3	10.1	1:3	0.027	7.3 ± 1.1	6.1 ± 0.9	1.2 ± 0.3
BT4	13.4	1:4	0.079	7.1 ± 1.1	5.3 ± 0.7	1.3 ± 0.3
BT5	16.8	1:5	0.239	7.8 ± 2.5	5.0 ± 0.8	1.6 ± 0.5

[a] Boric acid amount (mmol) used in the preparations, [b] Nominal TiO_2 : H_3BO_3 ratios, [c] B : Ti measured molar ratios, obtained by ICP-AES measurements, [d] TEM measurements. Mean value ± standard deviation σ; statistics on about 60 particles (nm), e Calculated long axis: short axis ratio.

Table 1. Details of boron-modified TiO_2 nanocrystals samples

XRD was carried out to investigate the crystal structure of boron-modified TiO_2 nanoparticles and the corresponding XRD patterns are shown in Figure 2.

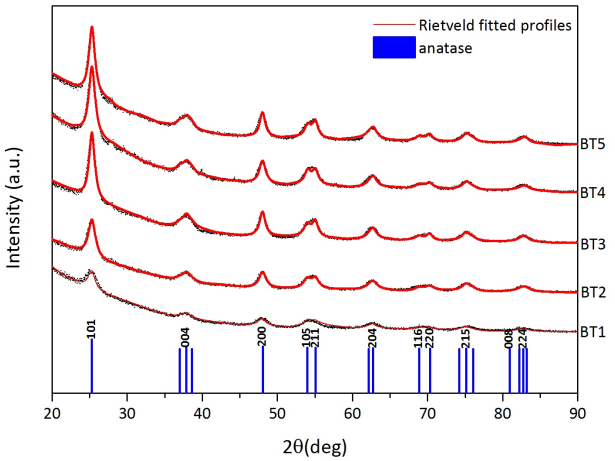

Figure 2. XRD patterns of TiO_2:(B)

Sample	a.s.r.[a]	Ti[b]	O[b]	004[c]	200[c]	a=b [Å^{-1}][d]	c [Å^{-1}][d]
BT1	1.04	1.07	2.49	5.07	5.29	3.785	9.492
BT2	1.22	0.99	2.44	4.60	5.63	3.786	9.492
BT3	1.39	0.98	2.42	4.90	6.84	3.786	9.492
BT4	1.41	0.99	2.26	4.32	6.08	3.785	9.481
BT5	1.52	1.00	2.10	4.66	7.09	3.785	9.478

[a] Aspect size ratio, [b] Occupancy, [c] Apparent size along the indicated directions (nm), [d] Anatase unit cell lattice parameters.

Table 2. XRD parameters of TiO_2:(B) nanocrystals

Table 2 summarizes the relevant data extracted from Rietveld analysis: titanium and oxygen lattice site occupancy, which were found to deviate slightly from the stoichiometric values of Ti = 1 and O = 2, the apparent size along the crystallographic [004] and [200] directions, respectively, along the rod length and the base diameter, from which the aspect size ratio was determined. The refined anatase lattice parameters, evidenced a c-axis contraction for high nominal boron concentrations, for high nominal boron concentrations as expected from results reported in previous papers [12, 18].

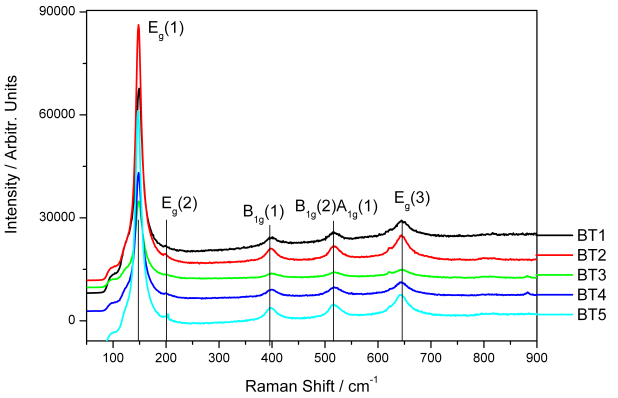

Figure 3. Raman spectra of nanocrystalline TiO_2:(B) samples.

Micro Raman spectra were collected on TiO_2:(B) samples and are reported in Figure 3. All the detected peaks in Raman spectra belong to the anatase TiO_2 phase and lie in the region 100–700 cm^{-1}: Fig. 3 shows E_g(1) around 144cm^{-1}, E_g(2) at 197 cm^{-1}, B_{1g}(1) at 400 cm-1, A_{1g}(1) and B_{1g}(2) at 520 cm^{-1}, and E_g(3) at 640 cm^{-1}.

Table 3 shows the data for unmodified and modified bricks, obtained varying suspensions weight percentages (from 0.5 wt.% to 2 wt.%). Tests have shown that nanocrystals increasing additions, under the error left the bulk density and the apparent density, water absorption and the apparent porosity were left almost unchanged. The resulting bulk densities were a little higher in respect to the reference brick. Bending failure tests were conducted on three points at room temperature, using a programmed press. Each dried specimen was placed horizontally between two supports distanced by 100 mm, and divided into two half prisms. Compression breakage tests were conducted according to standard regulations: the two prisms settled previously for the bending test were used, and in this case a press with a programmed control was also employed. The load was uniformly increased at a speed of 2400 N/s, until the specimen failure. The failure mode denoted fragile composites.

The breaking strength (Table 3) increased appreciably with the nanoadditive concentrations with respect to the reference brick. Thermal Diffusivity, determined by the hot disk method slightly decreased with nanofillers amount (Table 3).

Sample	Nanoadditive (wt.%)	Bulk density (g/cm^3)	Apparent density (g/cm^3)	Apparent porosity (%)	Water Absorption (%)	Breaking strength (MPa)	Diffusivity (mm^2/s)
Commercial composition brick		2.70± 0.05	2.28± 0.05	18.5± 0.5	8.1± 0.2	80.00± 0.01	1.06± 0.01
TiO_2 :(B) modified brick	0.5	2.81± 0.05	2.28± 0.05	19.0± 0.5	8.2± 0.2	86.55± 0.01	1.00± 0.01
	1	2.80± 0.05	2.30± 0.05	18.0± 0.5	7.8± 0.2	90.40± 0.01	0.88± 0.01
	2	2.78± 0.05	2.29± 0.05	17.7± 0.5	7.7± 0.2	97.60± 0.01	0.84± 0.01

Table 3. Thermo-physical and mechanical properties of aluminosilicate bricks showing only bands corresponding to the anatase TiO_2 Raman modes, as described in the text.

Sample	Nanoadditive (wt.%)	Cumulative volume (cc/g)	Surface area (m^2/g)	Pores size (μm)	Open Porosity (%)
Commercial composition brick		0.098± 0.005	1.04± 0.01	0.35± 0.02	20.84± 0.06
TiO_2 :(B) modified brick	0.5	0.083± 0.005	1.49± 0.01	0.36± 0.02	19.77± 0.06
	1	0.085± 0.005	1.53± 0.01	0.45± 0.02	19.82± 0.06
	2	0.086± 0.005	1.57± 0.01	0.50± 0.02	19.94± 0.06

Table 4. Surface areas, total volume, pore dimensions, and open porosity of commercial composition versus nanocrystals modified bricks.

Results reported in Table 4 show that the cumulative volume, which is indicative of the matrix compactness, does not correlate with the nanocrystals' amounts and is only slightly lower than in the reference brick. The surface areas increased as well as the calculated pores' size, while the calculated open porosity was lower than in the reference brick (which is in agreement with results reported in Table 3). To study the mechanism improving the breaking strength, SEM analysis of refractory bricks has been conducted and the microstructures at low and high magnification are shown in Fig. 4.

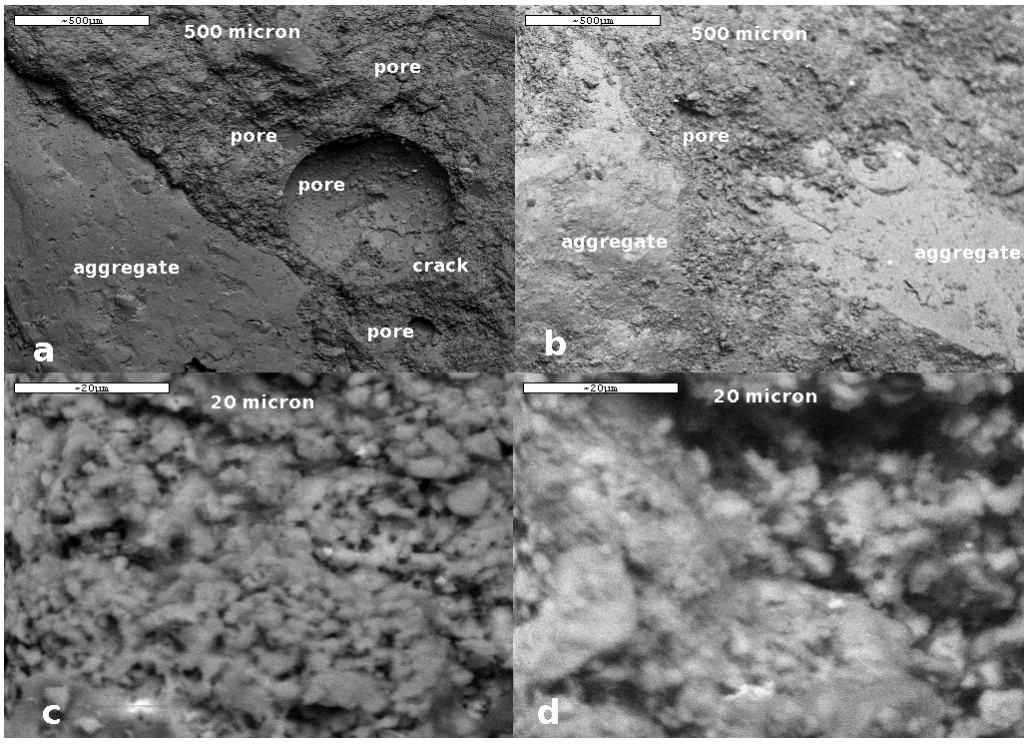

Figure 4. SEM images of bricks: (a), (c) without, and (b), (d) with TiO_2:(B) (2% wt) nanoparticles' addition.

In the low magnification mode, large aggregates with smooth surfaces could be observed in both samples; however, in the refractory without nanoparticles there are areas with clear internal defects and larger micropores. The addition of TiO_2:(B) nanoparticles causes some differences in the microstructures: the microcracks' and micropores' sizes were greatly reduced. High magnification SEM images confirmed a denser microstructure with fewer voids in TiO_2:(B) modified refractory (Fig. 4: c and d). Moreover, EDS through the elemental analysis evidenced that in nanocrystals-modified specimens the fillers were present along the entire scanned surface.

To explain SEM results and the overall increase in the breaking strength with nanocrystals' additions it is to be assumed that nanoadditives possibly induced a better particles' aggregation, through a thickening effect during the formation of the liquid phase. Previous literature studies [19] demonstrated that anatase containing boron, at least at the surface of the nanocrystals, has peculiar characteristics in bricks: boron favours the persistence of the anatase phase when thermal treatments are performed [19]. It can qualitatively explain the higher compression breaking resistance with the nanofillers obtained in the present study. The results of the SEM analysis are in contradiction with results collected in Table 4, where an increase in the pore radii calculated in bricks with modified nanocrystals is observed: we speculate that it may be because of a failure of the hypothesis of the Washburn equation, which is valid for cylindrical pores.

4. Conclusions

In the present work, a microwave-assisted synthesis of boron-modified TiO_2 anatase nanocrystals with about one minute and a half of reaction time was developed. The effective boron content was tuned by the addition of boric acid and increased with its nominal amount. It was found that boron addition does not influence appreciably the nanocrystals' size and morphology. One of the obtained samples was tested as additive in various quantities in a typical aluminosilicate refractory composition. The effects of nanocrystals' addition on bricks were evaluated according to UNI EN 196/2005 in terms of thermophysical, mechanical properties, and microstructure. The thermal conductivity decreases and breaking strength increases with the nanofillers' addition. According to SEM images the TiO_2:(B) nanoparticles' addition reduced the microcracks' and micropores' sizes.

SEM-EDS spectroscopy confirmed the presence of nano fillers along the scanned surfaces. Possibly, nanoadditives induced better particles' aggregation, through a thickening effect during the formation of the liquid phase; in this way the nanocrystals-modified bricks presented improved mechanical characteristics due to a better compaction of the components.

5. Acknowledgements

This work was partially supported by the FIRB 2009/2010 project "Rete integrata per la Nano Medicina (RINAME)" — RBAP114AMK_006. Giuseppe Chita and Giovanni Filograsso are acknowledged for their technical and administrative support.

PO FESR 2007-2013 - Regione Puglia Aiuti a sostegno dei partenariati regionali per l'innovazione NAno / MIcro STrutturazione nei materiali per l'Edilizia ed altri settori produttivi (NAMISTE). Cod. 2Y6DME5.

PON, Avviso prot. n. 84/Ric. del 2 marzo 2012 NAnoMAteriali per l'edilizia SosTEnibile (NAMASTE) prot. PON04a3_00107 CUP: B35I12000100005. PON 254/Ric. Potenziamento del "CENTRO RICERCHE PER LA SALUTE DELL'UOMO E DELL'AMBIENTE" Cod. PONa3_00334. CUP: F81D11000210007.

6. References

[1] Balkevich VL, Medvedovskaya EI, Popov ON, Orlova VN (1984) Contact interaction of bacor and silica refractories. Refractories and Industrial Ceramics 25:118–121.

[2] Arahori T, Suzuki T (1987) Transformation of tridymite to cristobalite below 1470° C in silica refractories. J Mater Sci 22:2248–2252.

[3] Brown JT, Wosinski JF, Alkali resistant silica refractory. (2001) US Patent 6, 313, 057.

[4] Chrzan ES, Petrie EC, Swain SM (1952) Study of silica brick from a glass tank crown. J American Ceramic Society 35:173–181.

[5] Coler SS (1930) Thermal expansion of silica brick and mortars. Journal of the American Ceramic Society 13:437–446.

[6] Houldsworth HS, Cobb JW (1923) The reversible thermal expansion of refractory materials. J American Ceramic Society 6:645–662.

[7] Austin JB, Pierce RHH (1933.) Constitution and thermal expansion of silica cokeoven brick after service. J Am Ceramic Soc 16:102–106.

[8] Yang Y, Wang Y, Tian W, Wang Z-Q, Zhao Y, Wang Y, Bian H-M (2009) Reinforcing and toughening alumina/titania ceramic composites with nano-dopants from nanostructured composite powders. Mat Sci Engineering A 508:161–166.

[9] Manivasakan P, Rajendran V, Rauta P R, Sahu B B, Sahu P, Panda B K, Valiyaveettill S, Jegadesan S (2010) Effect of TiO_2 nanoparticles on properties of silica refractory. J American Ceramic Society 93:2236–2243.

[10] Huang C-L, Wang J-J, Huang C-Y (2007) Microwave dielectric properties of sintered alumina using nano-scaled powders of α alumina and TiO_2. J American Ceramic Society 90:1487–1493.

[11] Carlucci C, Scremin BF, Sibillano T, Giannini C, Filippo E, Perulli P, Capodilupo AL, Corrente GA, Ciccarella G (2014) Microwave-assisted synthesis of boron-modified TiO_2 nanocrystals.Inorganics 2:264–277.

[12] Xu H, Picca RA, De Marco L, Carlucci C, Scrascia A, Papadia P, Scremin BF, Carlino E, Giannini C, Malitesta C, Mazzeo M, Gigli G, Ciccarella G (2013) Nonhydrolytic route to boron-doped TiO_2 nanocrystals. Eur J of Inorg Chem 3: 364–374.

[13] Carlucci C, Xu H, Scremin BF, Giannini C, Altamura D, Carlino E, Videtta V, Conciauro F, Gigli G, Ciccarella G (2014) Selective synthesis of TiO_2 nanocrystals with morphology control with the microwave-solvothermal method. Cryst Eng Comm 16:1817–1824.

[14] Carlucci C, Xu H, Scremin BF, Giannini C, Sibillano T, Carlino E, Videtta V, Gigli G, Ciccarella G (2014) Controllable One-Pot Synthesis of Anatase TiO_2 Nanorods with the Microwave-Solvothermal Method. Sci Adv Mater 6:1668–1675.

[15] Xu H, Carlucci C, Scremin BF, Giannini C, Sibillano T, Scrascia A, Capodilupo AL, Gigli G, Ciccarella G (2014) Synthesis of ultrafine anatase titanium dioxide TiO_2 nanocrystals by the microwave-solvothermal method. J Nanoeng Nanomanufact 4:28–32.

[16] FULLPROF Refinement of powder (Rietveld) and single-crystal diffraction data Accessed 22 September 2014 http://www.ill.eu/sites/fullprof.

[17] Washburn EW (1921) The dynamics of capillary flow. Phys Rev 17:273–283.

[18] Chen D, Yang D, Wang Q, Jiang Z (2006) Effects of Boron Doping on Photocatalytic Activity and Microstructure of Titanium Dioxide Nanoparticles. Industrial & Engineering Chemistry Research 45: 4110–4116.

[19] Imteyaz Ahmad Md, Bhattacharya SS, Hahn H (2009), Thermal stability, and optical properties of boron modified nanocrystalline anatase prepared by chemical vapor synthesis. Journal of Applied Physics 105:113526–113534.